Zhang *et al*. *J Mater Inf* 2024;4:1
DOI: 10.20517/jmi.2023.34

Journal of Materials Informatics

Research Article

Open Access

High hydrogen evolution activities of dual-metal atoms incorporated N-doped graphenes achieved by coordination regulation

Cunjin Zhang, Shuaibo Qin, Hui Gao, Peng Jin*

School of Materials Science and Engineering, Hebei University of Technology, Tianjin 300130, China.

***Correspondence to:** Prof. Peng Jin, School of Materials Science and Engineering, Hebei University of Technology, No. 5340, Xiping Road, Beichen District, Tianjin 300130, China. E-mail: pengjin@hebut.edu.cn

How to cite this article: Zhang C, Qin S, Gao H, Jin P. High hydrogen evolution activities of dual-metal atoms incorporated N-doped graphenes achieved by coordination regulation. *J Mater Inf* 2024;4:1. https://dx.doi.org/10.20517/jmi.2023.34

Received: 31 Oct 2023 **First Decision:** 24 Nov 2023 **Revised:** 13 Dec 2023 **Accepted:** 27 Dec 2023 **Published:** 3 Jan 2024

Academic Editors: Jingxiang Zhao, Xingjun Liu, Fengyu Li **Copy Editor:** Dong-Li Li **Production Editor:** Dong-Li Li

Abstract

Electrolysis of water to produce hydrogen (H) can solve the current energy crisis and environmental problems. However, efficient hydrogen evolution reaction (HER) catalysts are still limited to a few noble metals, thus prohibiting their broad applications. Herein, first-principles calculations were carried out to investigate the theoretical HER performances of a series of N-doped graphenes containing inexpensive single- and dual-metal atoms. Among them, MN_4-gra (M = Fe, Co, Ni), homonuclear MMN_6-gra, and heteronuclear $M1M2N_6$-gra mostly exhibit low HER activities due to the weak H adsorption, and only CoN_4-gra, $NiNiN_6$-gra, and $CoNiN_6$-gra show better ΔG_{*H} values of 0.19, 0.15 and 0.27 eV, respectively. In contrast, low-coordinated MMN_5-gra and $M1M2N_5$-gra both have rather high HER activities. In particular, the ΔG_{*H} values of $FeNiN_5$-gra and $CoNiN_5$-gra are as low as -0.04 and -0.06 eV, respectively, very close to the ideal 0 eV. Detailed analyses reveal that such high activity mainly stems from the reduced metal coordination and the synergistic effect between the two metals, which greatly enhance the adsorption ability of the active center. More interestingly, the strong H adsorption of MMN_5-gra/$M1M2N_5$-gra could enable them to further adsorb a second H atom and generate a stable HMH intermediate to yield the final product H_2. Under this novel mechanism, the two-step $|\Delta G_{*H}|$ values of $FeNiN_5$-gra and $CoNiN_5$-gra are all no more than 0.10 eV. Our work not only discloses the important effect of coordination regulation and site synergy on enhancing the catalytic activity but also finds a new HER path on the metal-embedded N-doped graphenes.

Keywords: Hydrogen evolution reaction, density functional calculations, N-doped graphene, dual-atom catalyst, coordination regulation

INTRODUCTION

The massive consumption of fossil resources and the increasingly serious environmental problems prompt people to search for suitable alternative energy sources and develop efficient energy conversion technologies. However, the lack of cheap and high-efficiency catalysts largely restricts the overall efficiency of energy conversion devices and is the main bottleneck for realizing the transformation of energy supply forms. As important chemical reactions, hydrogen evolution reactions (HER) and oxygen evolution reactions (OER) form the whole reaction of water electrolysis to produce hydrogen (H)[1-4]. The generated hydrogen can then be used in fuel cells as a carrier of clean energy due to its high mass energy density[5-7]. Unfortunately, the current utilization of hydrogen energy is still in its infancy due to the lack of cheap and efficient HER catalysts. As an optimal HER catalyst, platinum (Pt) requires only negligible overpotentials in acidic solutions to achieve high reaction rates[8-11]. However, the scarcity limits its large-scale application. Although many HER catalysts such as transition-metal phosphides[12-14], carbides[15-17] and sulfides[18,19] have been developed, the excellent performance as that of Pt/C is still hard to achieve.

In recent years, single-atom catalysts (SACs), exemplified by the metal atoms anchored on nitrogen (N)-doped graphenes (M-N-C), exhibit excellent catalytic activities in many important electrocatalytic processes[20-22]. The unique structure of SACs achieves nearly 100% atomic utilization and excellent catalytic performance[23-25]. Thus, they become promising catalyst materials for HER[26-32]. For example, Lu *et al.* prepared a Ru and N co-doped carbon material (RuC_xN_y) as an efficient HER catalyst[33]. When the overpotential is only -12 mV, the current density can reach 10 mA·cm^{-2}, and the catalytic performance is significantly better than that of commercial Pt-based catalysts. Its excellent catalytic activity is mainly attributed to the embedded Ru atoms in the carbon matrix. First-principles calculations indicate that RuC_xN_y has a lower hydrogen binding energy and a lower dissociation kinetics energy barrier than the Ru nanoparticles.

Compared with SACs, dual-atom catalysts (DACs) not only maintain the high atomic utilization and good selectivity and stability but also have higher metal loading and more complex and flexible active sites. The possible synergistic effect, orbital coupling, and electron redistribution between adjacent metal centers and their functionality complementarity provide more opportunities for better catalytic performance[34-36]. Thus, they have attracted more interest than SACs. For example, Zheng *et al.* constructed a series of N-doped porous graphene (NPG)-based diatomic catalysts MM'-NPG and studied their HER activity[37]. Due to the dual active centers and controllable electronic structure, FeV-NPG and NiV-NPG could replace the noble metal HER catalysts under alkaline conditions. Zhou *et al.* synthesized the Rh-Fe dual atoms-embedded N-doped carbon hollow spheres, which exhibit a low overpotential of 36 mV for HER due to the electron redistribution promoted by Fe on the active Rh site[38]. Zhao *et al.* reported that the presence of C_1-Pt-Ru-N_2 structures in Pt_1Ru_1/NMHCS-A (activated N-doped mesoporous hollow carbon spheres) can greatly accelerate the H_2 generation with a rather low overpotential of 22 mV to achieve a current density of 10 mA·cm^{-2}[39]. However, the formation of atomic-scale metal sites without obvious aggregation remains as a large challenge for DACs. On the other hand, the coordination environment of the catalyst active center also greatly affects the H adsorption and desorption. By carefully adjusting the coordination environment of the active center, the performance of the catalyst can be further improved[40].

To obtain potential HER catalysts, we herein constructed a series of single-/dual-metal atom-incorporated N-doped graphenes with different coordination environments and systematically investigated their HER activities by density functional theory (DFT) calculations. The potential active centers of various catalysts and the adsorption structures of the key *H intermediate were investigated in detail. The HER activity of each catalyst was evaluated by calculating the free energy of H adsorption, and some very promising HER catalysts were then proposed. Finally, in-depth electronic structure analyses revealed the activity origins of the catalysts to provide a theoretical guide for the rational design of related catalytic materials.

COMPUTATIONAL METHODS

DFT calculations considering spin polarization were carried out by using the Vienna *ab initio* simulation package (VASP)[41]. The Perdew-Burke-Ernzerhof (PBE)[42] functional and the projector augmented wave (PAW) method are used. The dispersion interactions during adsorption were considered by using the popular Grimme's DFT-D3 correction method[43]. The convergence thresholds are 10^{-5} eV and 0.02 eV/Å for the energy and force, respectively, and the cutoff energy for the plane wave basis set is 500 eV. A vacuum space of 15 Å was applied along the z-direction to avoid the interactions between slabs. A 2 × 2 × 1 Monkhorst-Pack k-point mesh was used because the cell is as large as 17.22 Å × 17.22 Å × 15.04 Å. All these parameters have been carefully tested in our recent work[44]. All the results were visualized with the aid of the VESTA software[45].

To evaluate the structural stability of metal atoms in the N-doped graphene, the formation energy (taking low-coordinated ones as an example) was calculated as:

$$E_f = E_{MN3\text{-gra}} - E_{N3\text{-gra}} - E_M \quad (1)$$

or

$$E_f = E_{MMN5\text{-gra}} - E_{N5\text{-gra}} - 2E_M \quad (2)$$

where $E_{MN3\text{-gra}}$ and $E_{N3\text{-gra}}$ are the calculated energies of SACs and corresponding N-doped graphene without the metal atom, respectively. Similarly, $E_{MMN5\text{-gra}}$ and $E_{N5\text{-gra}}$ are the homonuclear DAC and corresponding metal-free structures, respectively. E_M denotes the calculated energy of a metal atom in its stable bulk structure. Therefore, a more stable metal site has a more negative E_f value.

The adsorption Gibbs free energies were calculated as:

$$\Delta G = \Delta E + \Delta ZPE - T\Delta S \quad (3)$$

where the adsorption energies of the first and second H atoms are calculated as $\Delta E_{*H1} = E_{*H1} - E_{*} - 1/2E_{H2}$ and $\Delta E_{*H2} = E_{*H2} - E_{*H1} - 1/2E_{H2}$, respectively. E_{*H1} and ΔE_{*H2} are the energies of the systems with one and two adsorbed H atoms, respectively. E_{*} is the energy of the catalyst. E_{H2} is the energy of a free H_2 molecule. ΔZPE is the change in zero-point energy upon adsorption, while ΔS represents the change in entropy. They were obtained from the vibrational frequency calculations and standard thermodynamic data, as done in the recent literature[46]. T is the temperature (298.15 K). We assume pH = 0 and applied potential U = 0 V *vs.* Standard hydrogen electrodes (SHE) in the calculations. The computational hydrogen electrode (CHE) model[47] was used to calculate the Gibbs free energy change, namely assuming the free energy of an isolated H_2 molecule is twice that of a proton-electron pair. For simplicity, the hydrogen coverage was not considered, and it is assumed to have a negligible effect as it does on other catalyst surfaces[46].

RESULTS AND DISCUSSION

MN_4-gra/MMN_6-gra/$M1M2N_6$-gra

We first investigated the nine MN_4-gra (M = Fe, Co, Ni), MMN_6-gra, and $M1M2N_6$-gra catalysts, and Figure 1 gives their typical structures with each metal surrounded by four N atoms. Our recent study revealed that some MMN_6-gra and $M1M2N_6$-gra catalysts exhibit excellent OER activity due to the rich site synergy effects[44]. They are all planar, and their structural stabilities have been confirmed. Herein, we turned to investigate their possible HER activities.

In the acidic solution (pH = 0), the abundant H^+ in the electrolyte can be adsorbed on the catalyst under a certain external voltage to form a *H-rich surface, which then reacts to generate hydrogen molecules. Therefore, it is important to study the adsorption behavior of hydrogen on the catalyst surface, with the free energy change (ΔG_{*H}) of the adsorption process being the most critical activity descriptor of a HER catalyst[8]. The ideal catalyst should have a zero ΔG_{*H} value as a result of balanced adsorption and desorption. Figure 1 shows all possible H adsorption sites of these catalyst models. The geometric optimization of the H adsorption configuration on their surfaces was carefully performed to ensure that the most favorable H adsorption structure and adsorption site were found for each of them. Note that besides the metal and carbon sites considered in our recent OER study[44], the N atoms coordinating with metals were also included in this work because they are widely regarded as potential HER active centers[33,37,48]. Supplementary Tables 1-9 summarize the adsorption structures and corresponding ΔG_{*H} values on all these active sites of the above nine catalysts.

First, for the metal sites, the hydrogen atom tends to be vertically adsorbed on most metals except that the one on the Ni site of $FeNiN_6$-gra is slightly close to the Fe site. The adsorption behavior of hydrogen on metal sites is basically consistent with the d-band center theory[49]. Compared with FeN_4-gra, the adsorption at Fe sites of $FeFeN_6$-gra, $FeCoN_6$-gra, and $FeNiN_6$-gra is weakened due to the formation of M-M bonds and the lowered metal d-band center (ε_d, Supplementary Table 10). They, thus, show lower HER catalytic activity ($\Delta G_{*H} \geq 0.37$ eV) than FeN_4-gra (ΔG_{*H}: 0.34 eV). Consistent with the d-band center order of Co atoms (CoN_4-gra > $CoNiN_6$-gra > $FeCoN_6$-gra > $CoCoN_6$-gra)[44], their corresponding ΔG_{*H} values are 0.19, 0.62, 0.79, and 0.84 eV, respectively. Among them, CoN_4-gra has the best HER catalytic activity with ΔG_{*H} of only 0.19 eV, which is well consistent with its high activity in recent experiments[48]. Interestingly, the hydrogen atom tends to adsorb on the non-metal sites (N or C sites) of NiN_4-gra instead of the Ni site. Compared with NiN_4-gra, the Ni site on $NiNiN_6$-gra exhibits enhanced H adsorption owing to its upshifted d-band center. Nevertheless, its H adsorption is still weak (ΔG_{*H}: 1.34 eV). The Ni sites of $FeNiN_6$-gra and $CoNiN_6$-gra exhibit weaker H adsorption due to the relatively strong Fe-Ni and Co-Ni interactions and the downshifted d-band center of Ni atoms. Thus, the Ni sites on these catalysts may be unsuitable for HER.

Then, all the non-metal active sites, namely the N atoms coordinating with metals and the C atoms coordinating directly with N atoms, were investigated. Supplementary Tables 1-9 show that besides the vertical adsorption on top of the N atom, the hydrogen atom on the N site may also reside slightly towards the metal site in some cases. The H adsorption strengths of N sites in different coordination environments are quite different. The N sites on MN_4-gra have weak H adsorption ($\Delta G_{*H} \geq 1.05$ eV, Figure 2), implying their low HER activity. For the N sites with two different coordination environments (N1, N2) on MMN_6-gra, the ΔG_{*H} of the N2 site is always smaller than that of the N1 site. It is worth noting that the ΔG_{*H} value at the N2 site of $NiNiN_6$-gra is only 0.15 eV, much lower than that of the Ni site (1.34 eV). Such a moderate H adsorption behavior suggests that the reaction could preferentially occur at this site, accompanied by a rather low ΔG_{*H} value (0.15 eV). Similarly, for $M1M2N_6$-gra, the N2 site directly coordinated with two metal atoms also has a strong H adsorption capacity. The ΔG_{*H} value for the N2 site

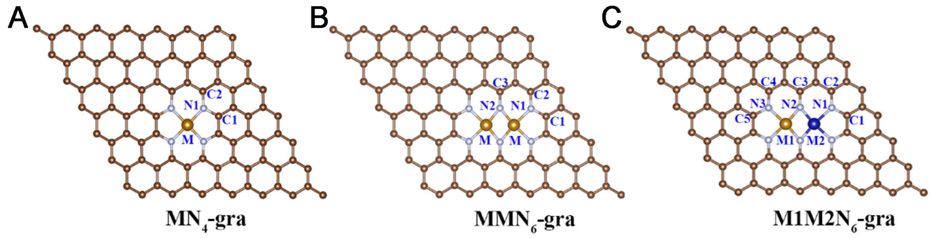

Figure 1. Potential active centers of each type of catalyst. (A) MN$_4$-gra (M = Fe, Co, Ni); (B) MMN$_6$-gra; (C) M1M2N$_6$-gra.

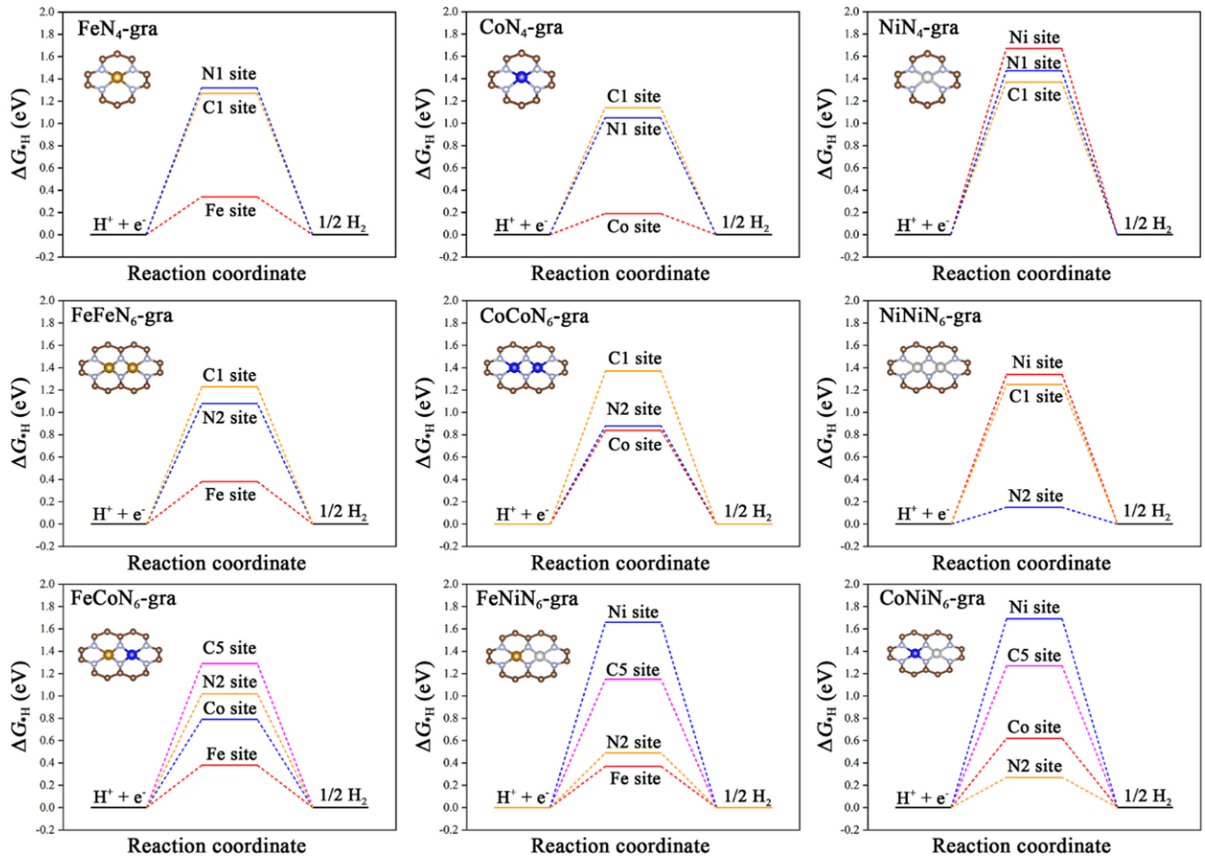

Figure 2. Gibbs free energy of H adsorption (ΔG_{*H}) at different sites on MN$_4$-gra/MMN$_6$-gra/M1M2N$_6$-gra. For the non-metal sites, only the values with the strongest adsorption are shown. Carbon: brown; Iron: golden; Cobalt: dark blue; Nickel: silvery; Nitrogen: light blue.

on CoNiN$_6$-gra is 0.27 eV, much smaller than that of the Co site (0.62 eV) and the Ni site (1.69 eV). For all the C sites, however, hydrogen atoms are always vertically adsorbed on their top, and the adsorptions are all weak ($\Delta G_{*H} \geq 1.14$ eV), indicating that the C sites of all catalysts are inactive for catalyzing HER.

In summary, the metal sites of the above catalysts mostly exhibit weak adsorptions, and only the Co site of CoN$_4$-gra shows potential high HER activity (ΔG_{*H}: 0.19 eV). For the same reason, all the carbon sites are unsuitable for HER. Interestingly, owing to the dual-atom doping, the N2 sites simultaneously coordinated with the two metal atoms present enhanced H adsorption. In particular, the moderate H adsorptions on these N sites render NiNiN$_6$-gra as a potential HER catalyst with ΔG_{*H} as low as 0.15 eV. The overall weak H adsorptions on the above catalysts [Figure 2] necessitate further tailoring of their structures to achieve better activity.

MN_3-gra/MMN_5-gra/$M1M2N_5$-gra

Theoretically, the HER performance of the above catalysts could be improved by reducing the number of coordinating N atoms because it will endow the central metal with a stronger coordination ability to enhance its H adsorption. We then constructed a series of SACs and DACs with three N atoms around each metal: MN_3-gra, MMN_5-gra, and $M1M2N_5$-gra[50,51]. However, the metal atoms in MN_3-gra (M = Fe, Co, Ni) SACs all protrude from the catalyst surface upon structural optimization [Supplementary Figure 1]. The formation energies of MN_3-gra are also positive, suggesting that they may be unstable and unsuitable for electrocatalytic reactions.

By comparison, the optimized structures of MMN_5-gra/$M1M2N_5$-gra DACs are all basically planar [Figure 3], with each metal atom well incorporated in the graphene plane. The metal atom and three nearby N atoms have average distances between 2.03~2.14 Å, all close to the sum of the covalent atomic radii [Supplementary Table 11]. This structural feature suggests that M-N covalent bonds may be formed, which are supported by the electron localization functions (ELFs), where substantial electron accumulation was found in the M-N regions [Supplementary Figure 2]. Consistently, the formation energies of these DACs are all negative (-0.61 to -0.06 eV), further confirming their energetic stabilities [Figure 3]. Moreover, the distances between two metal neighbors are all smaller than their covalent radii sum [Supplementary Table 11], indicating that M-M covalent bonds are formed, which are consistent with the ELF results in Supplementary Figure 2. The crystal orbital Hamiltonian population (COHP, Supplementary Figure 3) reveals that there are strong M-M bonding interactions under the Fermi level, which are largely due to the σ-type overlap of the metal $3d_{x2-y2}$ orbitals [Supplementary Table 12]. The large and negative integral-COHP (ICOHP) values of -5.03, -3.70, -2.74, -4.36, -3.15, and -2.97 for Fe-Fe, Co-Co, Ni-Ni, Fe-Co, Fe-Ni, and Co-Ni, respectively, further support the formation of M-M bonds. The metal atoms all donate some electrons to the N-doped graphene, as indicated by the charge density difference and Bader charges [Supplementary Figure 4].

The electronic properties were then investigated by the density of states (DOSs) and electronic band structures. As shown in Supplementary Figure 5, substantial hybridization was observed between the N-2*p* state and the M-3*d* state. Compared with MMN_6-gra/$M1M2N_6$-gra, the metal d-band centers (ε_d) in MMN_5-gra/$M1M2N_5$-gra all shift to higher energy levels [Supplementary Figure 5]. This difference can be understood from the lifted energy level of the metal $3d_{x2-y2}$ orbitals in projected DOSs (PDOS, Supplementary Figure 6). Meanwhile, the metals also exhibit lower spin states [Supplementary Figure 6]. In addition, there are rich electronic states around the Fermi level with small band gaps of 0 to 0.04 eV (Supplementary Figure 7; note that the gaps are generally underestimated at the PBE level). Thus, rapid electron transfer between the catalyst surface and the adsorbates is expected to speed up the electrocatalytic reaction.

The changed electronic structure caused by the reduced metal coordination number will inevitably affect the adsorption of *H. Supplementary Tables 13-18 summarize the adsorption structures and corresponding ΔG_{*H} on different active sites of all these low-coordinated DACs. For the metal sites, the H atom prefers to adsorb on the bridge site between two metal atoms of MMN_5-gra/$M1M2N_5$-gra as compared to a single metal site on MMN_6-gra/$M1M2N_6$-gra. Owing to such a novel dual-atom synergy, the ΔG_{*H} values decrease significantly [Figure 4] and are very close to 0 eV on the metal sites of $FeFeN_5$-gra (-0.16 eV), $FeCoN_5$-gra (-0.18 eV), $FeNiN_5$-gra (-0.04 eV), and $CoNiN_5$-gra (-0.06 eV). Thus, they, especially $FeNiN_5$-gra (ΔG_{*H}: -0.04 eV) and $CoNiN_5$-gra (ΔG_{*H}: -0.06 eV), may exhibit high catalytic activity.

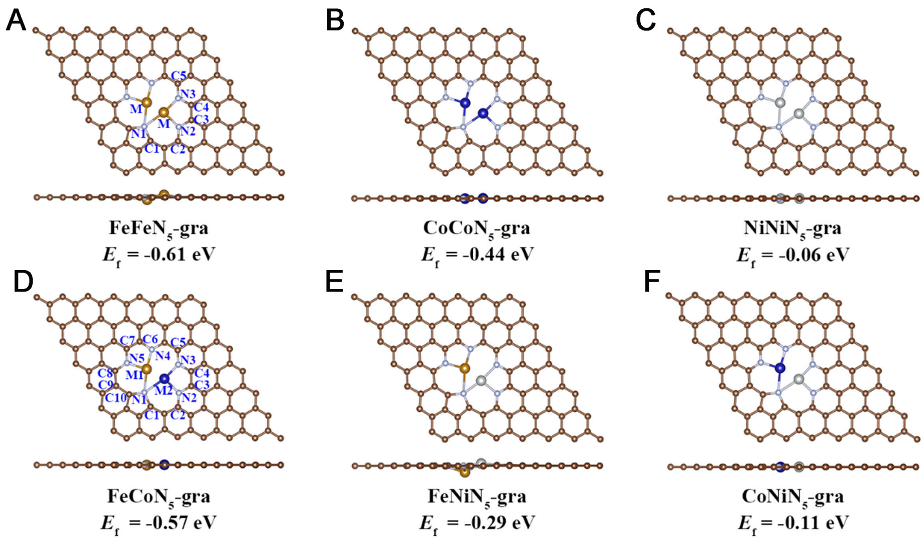

Figure 3. Optimized structures (two views) and formation energies (E_f) of (A-C) MMN_5-gra (M = Fe, Co, Ni) and (D-F) $M1M2N_5$-gra. The first column gives the different active sites considered for each kind of catalyst.

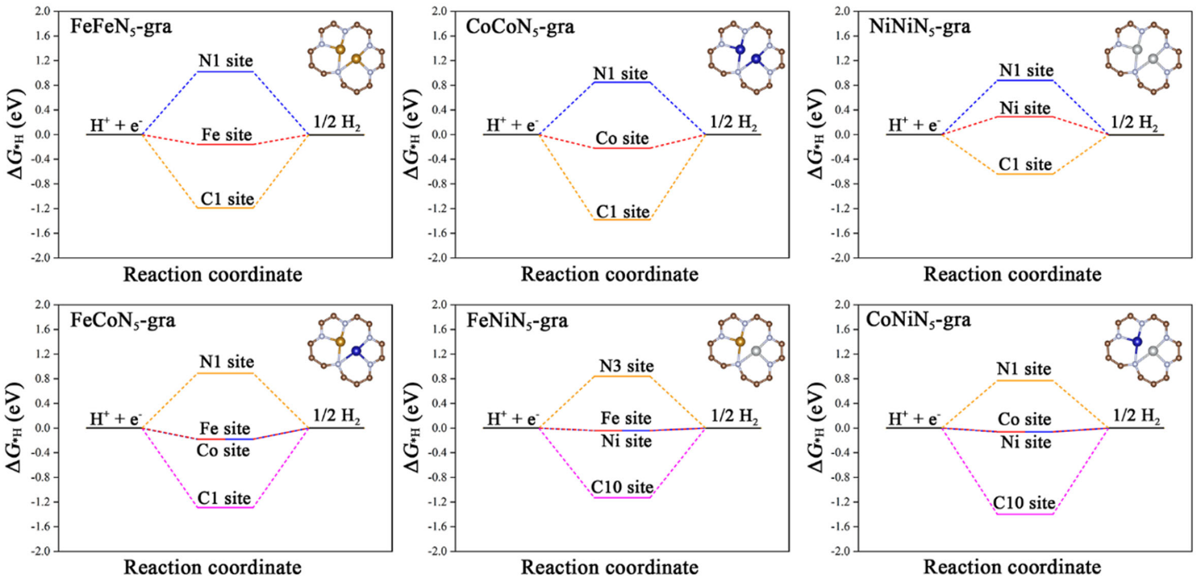

Figure 4. Gibbs free energy of H adsorption (ΔG_{*H}) at different sites on MMN_5-gra/$M1M2N_5$-gra. For the non-metal sites, only the values with the strongest adsorption are shown.

For the C sites, their overall adsorptions are still weak because their coordination environments in MMN_5-gra/$M1M2N_5$-gra are not significantly changed compared with MMN_6-gra/$M1M2N_6$-gra. Note that the C1 site of MMN_5-gra and the C1/C10 sites of $M1M2N_5$-gra exhibit strong H adsorption ($\Delta G_{*H} \leq -0.64$ eV, Figure 4) due to the deformation of the catalyst structure during the H adsorption. For the N sites, although, such as MMN_6-gra/$M1M2N_6$-gra, the N sites coordinated to two metals (i.e., N1 sites) in MMN_5-gra/$M1M2N_5$-gra mostly have the strongest H adsorption capacity, they are still weak ($\Delta G_{*H} \geq 0.77$ eV), not suitable for catalyzing HER. In summary, with rather low $|\Delta G_{*H}|$ values of less than 0.2 eV, $FeFeN_5$-gra, $FeCoN_5$-gra, $FeNiN_5$-gra, and $CoNiN_5$-gra are promising HER catalysts due to the high activity of their metal sites.

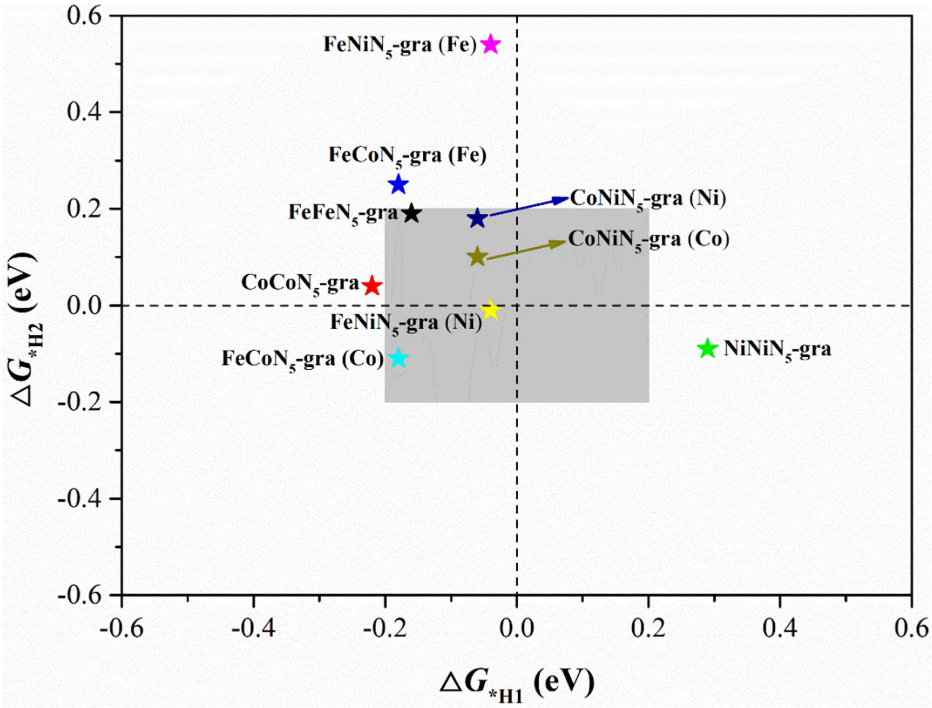

Figure 5. Adsorption Gibbs free energy of the first (ΔG_{*H1}) and second H (ΔG_{*H2}) in the HMH intermediates on different catalyst sites.

Dual-H co-adsorption path

When the metal coordination of the catalyst is unsaturated, the HER may also occur along a new reaction pathway[52-57]: after the formation of a usual MH species on the catalyst surface, a second H atom continues to be adsorbed on the same metal site to form a stable HMH intermediate. Thus, with low metal coordination numbers, the possibility for MMN_5-gra/$M1M2N_5$-gra to adsorb a second H atom was further investigated. The corresponding optimized structures are summarized in Supplementary Table 19. Indeed, all these catalysts formed stable HMH structures with one H atom on a metal and one H atom between two metals. The corresponding H-H distances are all no more than 1.86 Å. We calculated the adsorption free energy of the second H to evaluate its adsorption strength [Supplementary Table 20]. Most catalysts show favorable adsorption for the second H, especially the Ni site of $NiNiN_5$-gra (ΔG_{*H2} = -0.09 eV) and the Co site of $FeCoN_5$-gra (ΔG_{*H2} = -0.11 eV), suggesting that stable HMH structures could form on the surface of these catalysts.

Recently, Liberto *et al.* found that if the H_2 generation involves two reaction intermediates, MH and HMH, an excellent HER catalyst should be thermoneutral for every H adsorption[58,59]. Namely, the ΔG_{*H} values for both adsorption steps (ΔG_{*H1} and ΔG_{*H2}) should be close to 0 eV. We further evaluated the catalyst activity under this HER mechanism. As shown in Figure 5, $FeNiN_5$-gra may have the best activity under this mechanism via the adsorption at its Ni site. In addition, $CoNiN_5$-gra can achieve rather high catalytic activity either through Co sites (ΔG_{*H1}: -0.06 and ΔG_{*H2}: 0.10 eV) or through Ni sites (ΔG_{*H1}: -0.06 and ΔG_{*H2}: 0.18 eV). The other two promising candidates are $FeFeN_5$-gra and $FeCoN_5$-gra via their Fe and Co sites, respectively.

In conclusion, most of the MMN_5-gra/$M1M2N_5$-gra exhibited excellent HER activity through the MH intermediate reaction mechanism or through the HMH intermediate mechanism. In particular, the $|\Delta G_{*H}|$ values of $FeNiN_5$-gra and $CoNiN_5$-gra under both reaction mechanisms are all no more than 0.1 eV, indicating that they are potential HER catalysts. Supplementary Figure 8 depicts the calculated exchange currents for the above catalyst models based on their adsorption free energies. Among them, CoN_4-gra, $NiNiN_6$-gra, $FeNiN_5$-gra, CoNi-N_5-gra, $FeFeN_5$-gra, and $FeCoN_5$-gra reside much closer to the volcano peak with high activity.

Origins of HER activity

The above calculation results show that CoN_4-gra, $NiNiN_6$-gra, $CoNiN_6$-gra, and MMN_5-gra/$M1M2N_5$-gra all have better activities for catalyzing HER. However, the underlying reasons for their enhanced activities may be different.

For CoN_4-gra, its excellent HER activity can be attributed to the moderate adsorption of H on Co sites. To understand the huge difference in the H adsorption capacity of different metal sites, the charge transfer between metal atoms as HER active sites and adsorbed hydrogen atoms was further investigated. The charge density difference shows that charge accumulation (yellow area) mainly occurs on the adsorbed H atoms, whereas charge depletion (cyan area) is concentrated around the metal atoms [Supplementary Figure 9]. In addition, the results of Bader charge analysis show that the adsorption free energy of H increases with the decrease of the negative charge it carries; that is, the adsorption gradually weakens. For example, the negative charges carried by H on CoN_4-gra and $CoCoN_6$-gra are -0.07 and -0.03 [Figure 6A and B], respectively, and the adsorption free energies of H are correspondingly 0.19 and 0.84 eV.

The COHP between the metal atoms and the adsorbed H atoms was further calculated [Supplementary Figure 10]. The activation of H was also quantitatively assessed using the ICOHP. In general, a more negative ICOHP corresponds to a stronger H adsorption. For example, the Co-H interaction in CoN_4-gra (ICOHP: -3.28, Figure 6C) is much stronger than that in $CoCoN_6$-gra (ICOHP: -3.08, Figure 6D). A clear linear correlation between the ICOHP of M-H and the free energy of H adsorption for all MN_4-gra/MMN_6-gra/$M1M2N_6$-gra can be found in Figure 7A. This is also consistent with the above analyses that the downshifted d-band center of Co atoms in $CoCoN_6$-gra leads to the decreased H adsorption capacity of Co sites [Supplementary Table 10]. The DOS results also show slightly more obvious hybridization between the states of CoN_4-gra and adsorbed hydrogen [Figure 6C and D]. In addition, Figure 7B also plots the linear relationship between the metal d-band center and the H adsorption free energy, and the adsorption capacity of the metal site for H is in good agreement with the change of the d-band center.

The enhanced H adsorption capacity of MMN_5-gra/$M1M2N_5$-gra is consistent with the reduced coordination number and upshifted d-band center of the central metal [Supplementary Figure 5 and Supplementary Table 10]. Besides, the bridge site between two metals of MMN_5-gra/$M1M2N_5$-gra also helps to enhance their capture abilities. Further charge density difference and Bader charge analyses revealed that both metal atoms on MMN_5-gra/$M1M2N_5$-gra transfer electrons to the adsorbed H atoms, which results in a significant increase in the amount of charge on H (≤ -0.15, Figure 8) compared to the less negative charge of H on MMN_6-gra/$M1M2N_6$-gra (≥ -0.11, Supplementary Figure 9). In addition, according to the COHP analyses [Supplementary Figure 11], the bimetallic atoms on MMN_5-gra/$M1M2N_5$-gra simultaneously have bonding interactions with the adsorbed H atoms. This further confirms that the dual atoms in MMN_5-gra/$M1M2N_5$-gra both contribute to the H adsorption. Meanwhile, the excellent HER activity of MMN_5-gra/$M1M2N_5$-gra to generate H_2 through HMH intermediates can also be attributed to the enhancement of H adsorption capacity after reducing the coordination number of metal active centers and the synergistic effect of bimetallic site on H adsorption.

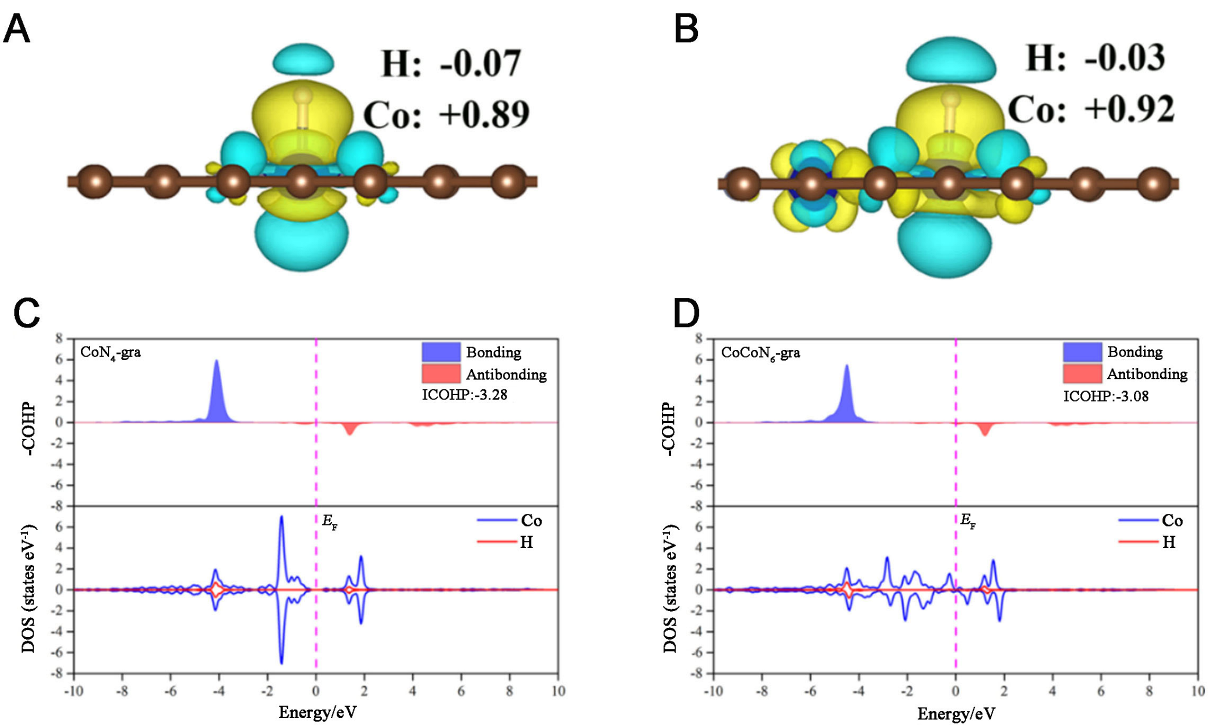

Figure 6. Charge density difference and Bader charge values during the hydrogen evolution reaction, (A) CoN_4-gra and (B) $CoCoN_6$-gra. COHP and DOS between M-H in *H of (C) CoN_4-gra and (D) $CoCoN_6$-gra. COHP: Crystal orbital Hamiltonian population; DOS: density of state.

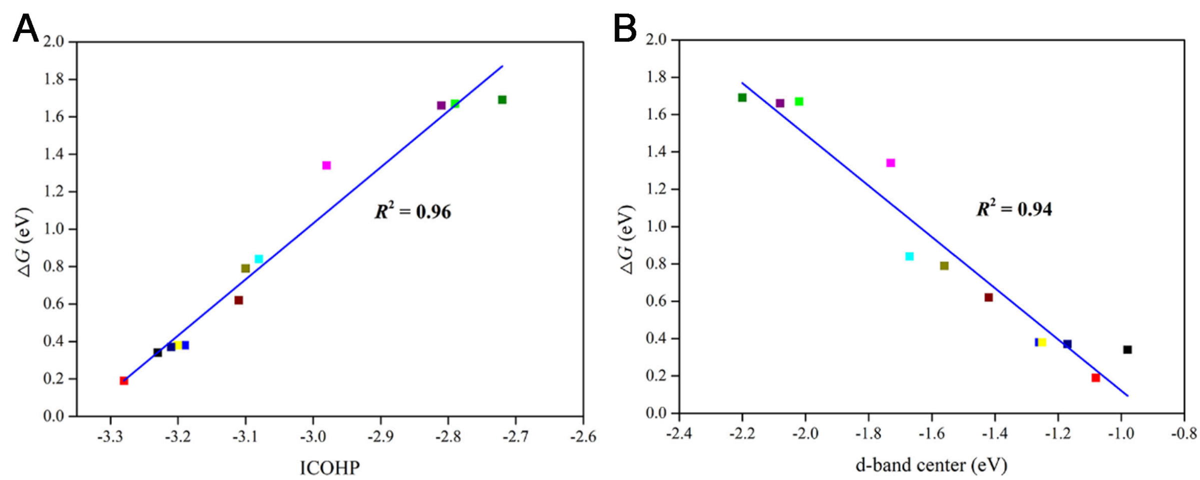

Figure 7. (A) Linear relationship between ICOHP and free energy of H adsorption for MN_4-gra/MMN_6-gra/$M1M2N_6$-gra; (B) Linear relationship between the d-band centers of the metals and free energy of H adsorption. ICOHP: M-H crystal orbital Hamiltonian population integral.

Finally, the HER activity of $NiNiN_6$-gra and $CoNiN_6$-gra is mainly due to the optimized electronic structure of the N2 site by doping bimetallic atoms. Specifically, the p-band center (ε_p)[60] of the N2 site in MMN_6-gra and $M1M2N_6$-gra is upshifted relative to that of MN_4-gra due to the direct coordination with two metal atoms [Figure 9]. This leads to a significant enhancement of the H adsorption capacity of N2 sites on MMN_6-gra and $M1M2N_6$-gra, especially $NiNiN_6$-gra (ε_p: -3.07 eV, ΔG_{*H}: 0.15 eV) and $CoNiN_6$-gra (ε_p: -3.43 eV, ΔG_{*H}: 0.27 eV). The charge density difference and Bader charge analyses reveal that, unlike the H

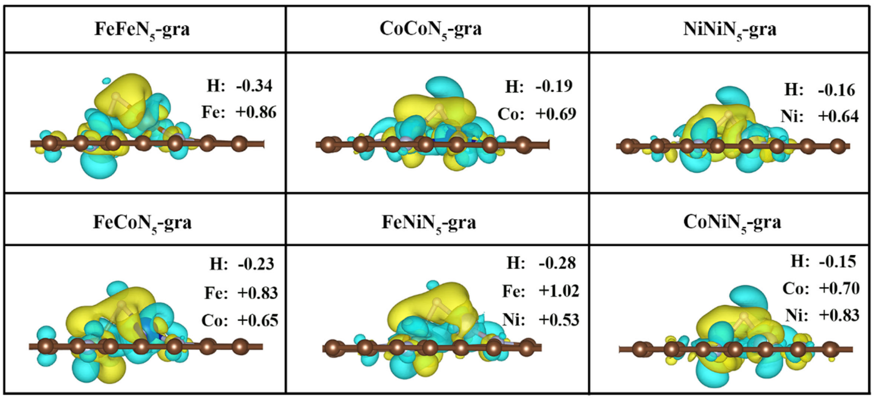

Figure 8. Charge density difference and Bader charge when the hydrogen evolution reaction occurs on the metal site for MMN$_5$-gra /M1M2N$_5$-gra.

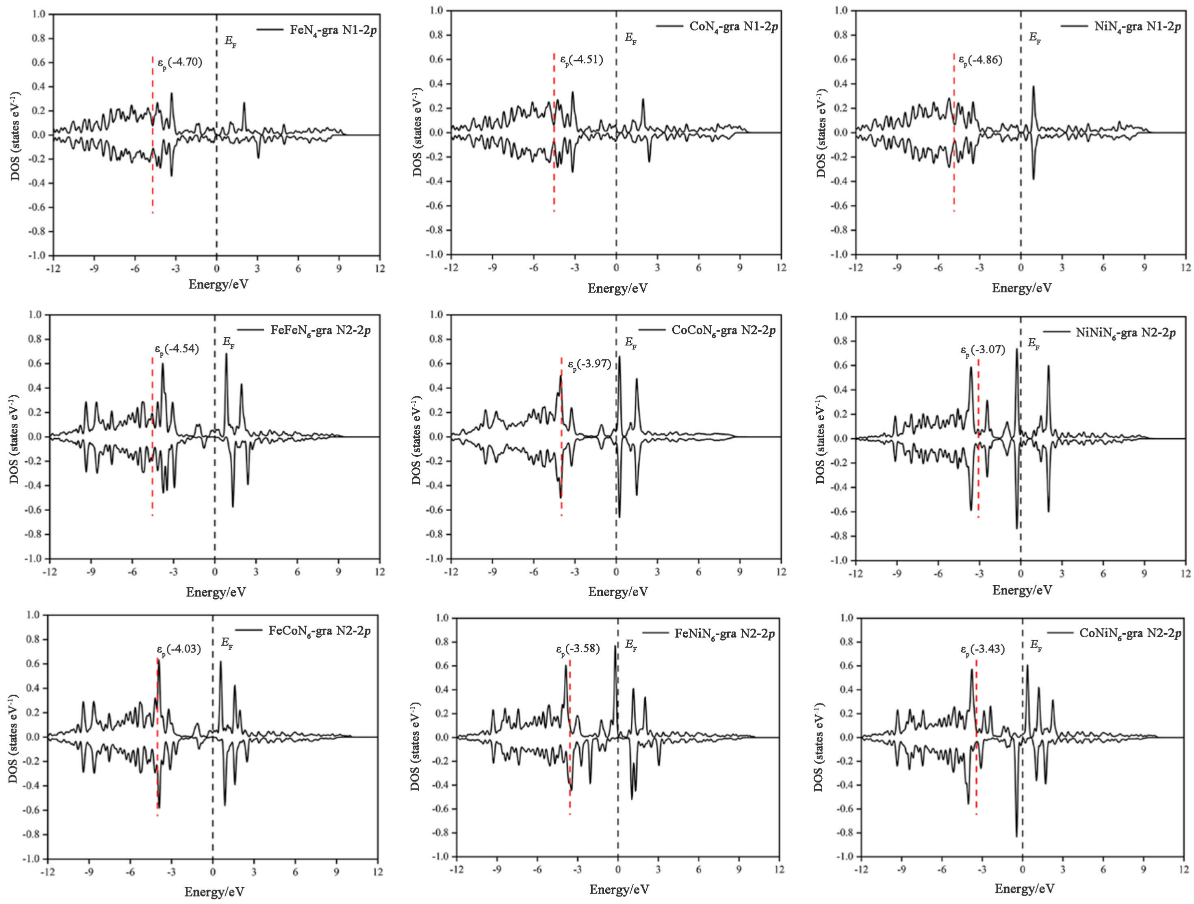

Figure 9. 2*p* projected density of states of N1 atoms in MN$_4$-gra and N2 atoms in MMN$_6$-gra/M1M2N$_6$-gra. DOS: Density of state.

adsorption on metal sites, the accumulation of charges mainly occurred around the N atoms, while the depletion of charge was mainly concentrated on the adsorbed H atoms [Supplementary Figure 12]. Moreover, when the N2 sites on NiNiN$_6$-gra and CoNiN$_6$-gra adsorb H, they have the largest amount of charge transfer, which are 0.44 and 0.43 e, respectively. Such massive electron transfer between N2 and H atoms leads to strong interactions between them. This is further confirmed by the COHP analysis of N-H, which has the most negative ICOHP of -7.29 and -7.23 on NiNiN$_6$-gra and CoNiN$_6$-gra, respectively [Supplementary Figure 13]. Similar to the linear relationship between ICOHP of M-H and H adsorption free energy, the ICOHP between N2-H on MMN$_6$-gra and M1M2N$_6$-gra also has a good linear relationship with the H adsorption free energy [Supplementary Figure 14A]. In addition, the linear relationship between the p-band center of the N2 atom and the free energy of H adsorption shows that the adsorption at the N2 site also follows the p-band center theory [Supplementary Figure 14B]. Overall, the optimization of the electronic structure of the N2 site due to the doping of bimetallic atoms enhances its H-trapping ability, which, in turn, improves the HER activity of NiNiN$_6$-gra and CoNiN$_6$-gra.

CONCLUSIONS

In summary, we investigated the HER activity of a series of SACs/DACs formed by embedding inexpensive Fe/Co/Ni atoms into N-doped graphene by systematic DFT calculations and found a variety of potential HER materials. Besides the CoN$_4$-gra, the ΔG_{*H} values of NiNiN$_6$-gra and CoNiN$_6$-gra are also as low as 0.15 and 0.27 eV, respectively. Reducing the coordination number of the metal in the active center can significantly enhance its H-trapping ability, and FeFeN$_5$-gra, FeCoN$_5$-gra, FeNiN$_5$-gra, and CoNiN$_5$-gra, thus, exhibit excellent HER catalytic activity with $|\Delta G_{*H}| \leq 0.18$ eV. Importantly, the reduced metal coordination of MMN$_5$-gra/M1M2N$_5$-gra and the synergy between metal atoms allow them to simultaneously adsorb two hydrogen atoms to form a stable HMH intermediate toward the final product H_2. Especially for FeNiN$_5$-gra and CoNiN$_5$-gra, both the $|\Delta G_{*H1}|$ and $|\Delta G_{*H2}|$ are $\leq$ 0.10 eV. The effective coordination regulation and site synergy revealed by this work provide deep insights into the HER process on diatomic catalysts and could guide the design of low-cost catalysts with activity comparable to noble-metal ones.

DECLARATIONS

Authors' contributions

Conceptualization, investigation, writing - original draft: Zhang C
Conceptualization, supervision, resources, writing - review and editing: Jin P
Investigation and data analysis and interpretation: Qin S, Gao H

Availability of data and materials

Not applicable.

Financial support and sponsorship

This work was supported by the National Natural Science Foundation of China (No. 22171068) and the Natural Science Foundation of Hebei Province (No. B2022202036).

Conflicts of interest

All authors declared that there are no conflicts of interest.

Ethical approval and consent to participate

Not applicable.

Consent for publication

Not applicable.

REFERENCES

1. Li L, Wang P, Shao Q, Huang X. Metallic nanostructures with low dimensionality for electrochemical water splitting. *Chem Soc Rev* 2020;49:3072-106. DOI
2. Jiao Y, Zheng Y, Jaroniec M, Qiao SZ. Design of electrocatalysts for oxygen- and hydrogen-involving energy conversion reactions. *Chem Soc Rev* 2015;44:2060-86. DOI PubMed
3. Huang J, Jiang Y, An T, Cao M. Increasing the active sites and intrinsic activity of transition metal chalcogenide electrocatalysts for enhanced water splitting. *J Mater Chem A* 2020;8:25465-98. DOI
4. Kim HJ, Kim HY, Joo J, et al. Recent advances in non-precious group metal-based catalysts for water electrolysis and beyond. *J Mater Chem A* 2022;10:50-88. DOI
5. Gray HB. Powering the planet with solar fuel. *Nat Chem* 2009;1:7. DOI PubMed
6. Liu M, Zhang R, Chen W. Graphene-supported nanoelectrocatalysts for fuel cells: synthesis, properties, and applications. *Chem Rev* 2014;114:5117-60. DOI
7. Majlan E, Rohendi D, Daud W, Husaini T, Haque M. Electrode for proton exchange membrane fuel cells: a review. *Renew Sust Energ Rev* 2018;89:117-34. DOI
8. Nørskov JK, Bligaard T, Logadottir A, et al. Trends in the exchange current for hydrogen evolution. *J Electrochem Soc* 2005;152:J23. DOI
9. Seh ZW, Kibsgaard J, Dickens CF, Chorkendorff I, Nørskov JK, Jaramillo TF. Combining theory and experiment in electrocatalysis: insights into materials design. *Science* 2017;355:eaad4998. DOI PubMed
10. Xu H, Cheng D, Cao D, Zeng XC. A universal principle for a rational design of single-atom electrocatalysts. *Nat Catal* 2018;1:339-48. DOI
11. Benck JD, Hellstern TR, Kibsgaard J, Chakthranont P, Jaramillo TF. Catalyzing the hydrogen evolution reaction (HER) with molybdenum sulfide nanomaterials. *ACS Catal* 2014;4:3957-71. DOI
12. Du H, Kong RM, Guo X, Qu F, Li J. Recent progress in transition metal phosphides with enhanced electrocatalysis for hydrogen evolution. *Nanoscale* 2018;10:21617-24. DOI PubMed
13. Sun J, Ren M, Yu L, et al. Highly efficient hydrogen evolution from a mesoporous hybrid of nickel phosphide nanoparticles anchored on cobalt phosphosulfide/phosphide nanosheet arrays. *Small* 2019;15:e1804272. DOI PubMed
14. Yan Q, Chen X, Wei T, et al. Hierarchical edge-rich nickel phosphide nanosheet arrays as efficient electrocatalysts toward hydrogen evolution in both alkaline and acidic conditions. *ACS Sustainable Chem Eng* 2019;7:7804-11. DOI
15. Gao Q, Zhang W, Shi Z, Yang L, Tang Y. Structural design and electronic modulation of transition-metal-carbide electrocatalysts toward efficient hydrogen evolution. *Adv Mater* 2019;31:1802880. DOI
16. Han N, Yang KR, Lu Z, et al. Nitrogen-doped tungsten carbide nanoarray as an efficient bifunctional electrocatalyst for water splitting in acid. *Nat Commun* 2018;9:924. DOI PubMed PMC
17. Zhou S, Zhou G, Jiang S, Fan P, Hou H. Flexible and refractory tantalum carbide-carbon electrospun nanofibers with high modulus and electric conductivity. *Mater Lett* 2017;200:97-100. DOI
18. Zhang B, Liu J, Wang J, et al. Interface engineering: The $Ni(OH)_2/MoS_2$ heterostructure for highly efficient alkaline hydrogen evolution. *Nano Energy* 2017;37:74-80. DOI
19. Ling Y, Yang Z, Zhang Q, Zhang Y, Cai W, Cheng H. A self-template synthesis of defect-rich WS_2 as a highly efficient electrocatalyst for the hydrogen evolution reaction. *Chem Commun* 2018;54:2631-4. DOI
20. Pan Y, Liu S, Sun K, et al. A bimetallic Zn/Fe polyphthalocyanine-derived single-atom Fe-N_4 catalytic site:a superior trifunctional catalyst for overall water splitting and Zn-air batteries. *Angew Chem Int Ed Engl* 2018;57:8614-8. DOI PubMed
21. Cao L, Luo Q, Chen J, et al. Dynamic oxygen adsorption on single-atomic Ruthenium catalyst with high performance for acidic oxygen evolution reaction. *Nat Commun* 2019;10:4849. DOI PubMed PMC
22. Varela AS, Ju W, Strasser P. Molecular nitrogen-carbon catalysts, solid metal organic framework catalysts, and solid metal/nitrogen-doped carbon (MNC) catalysts for the electrochemical CO_2 reduction. *Adv Energy Mater* 2018;8:1703614. DOI
23. Yao Y, Hu S, Chen W, et al. Engineering the electronic structure of single atom Ru sites via compressive strain boosts acidic water oxidation electrocatalysis. *Nat Catal* 2019;2:304-13. DOI
24. Wang X, Li Z, Qu Y, et al. Review of metal catalysts for oxygen reduction reaction: from nanoscale engineering to atomic design. *Chem* 2019;5:1486-511. DOI
25. Zhao Y, Zhou H, Chen W, et al. Two-step carbothermal welding to access atomically dispersed Pd_1 on three-dimensional zirconia nanonet for direct indole synthesis. *J Am Chem Soc* 2019;141:10590-4. DOI PubMed
26. Lei Y, Wang Y, Liu Y, et al. Designing atomic active centers for hydrogen evolution electrocatalysts. *Angew Chem Int Ed Engl* 2020;59:20794-812. DOI PubMed
27. Wang Y, Su H, He Y, et al. Advanced electrocatalysts with single-metal-atom active sites. *Chem Rev* 2020;120:12217-314. DOI PubMed
28. Zhuo HY, Zhang X, Liang JX, Yu Q, Xiao H, Li J. Theoretical understandings of graphene-based metal single-atom catalysts: stability

and catalytic performance. *Chem Rev* 2020;120:12315-41. DOI PubMed
29. Khalid M, Bhardwaj PA, Honorato AMB, Varela H. Metallic single-atoms confined in carbon nanomaterials for the electrocatalysis of oxygen reduction, oxygen evolution, and hydrogen evolution reactions. *Catal Sci Technol* 2020;10:6420-48. DOI
30. Fei H, Dong J, Arellano-Jiménez MJ, et al. Atomic cobalt on nitrogen-doped graphene for hydrogen generation. *Nat Commun* 2015;6:8668. DOI PubMed PMC
31. Qu Y, Chen B, Li Z, et al. Thermal emitting strategy to synthesize atomically dispersed Pt metal sites from bulk Pt metal. *J Am Chem Soc* 2019;141:4505-9. DOI
32. Xue Y, Huang B, Yi Y, et al. Anchoring zero valence single atoms of nickel and iron on graphdiyne for hydrogen evolution. *Nat Commun* 2018;9:1460. DOI PubMed PMC
33. Lu B, Guo L, Wu F, et al. Ruthenium atomically dispersed in carbon outperforms platinum toward hydrogen evolution in alkaline media. *Nat Commun* 2019;10:631. DOI PubMed PMC
34. Zhang L, Si R, Liu H, et al. Atomic layer deposited Pt-Ru dual-metal dimers and identifying their active sites for hydrogen evolution reaction. *Nat Commun* 2019;10:4936. DOI PubMed PMC
35. Bai L, Hsu CS, Alexander DTL, Chen HM, Hu X. A cobalt-iron double-atom catalyst for the oxygen evolution reaction. *J Am Chem Soc* 2019;141:14190-9. DOI PubMed
36. He T, Puente Santiago AR, Du A. Atomically embedded asymmetrical dual-metal dimers on N-doped graphene for ultra-efficient nitrogen reduction reaction. *J Catal* 2020;388:77-83. DOI
37. Zheng X, Yao Y, Ye W, Gao P, Liu Y. Building up bimetallic active sites for electrocatalyzing hydrogen evolution reaction under acidic and alkaline conditions. *Chem Eng J* 2021;413:128027. DOI
38. Zhou Y, Song E, Chen W, et al. Dual-metal interbonding as the chemical facilitator for single-atom dispersions. *Adv Mater* 2020;32:e2003484. DOI PubMed
39. Zhao W, Luo C, Lin Y, et al. Pt-Ru dimer electrocatalyst with electron redistribution for hydrogen evolution reaction. *ACS Catal* 2022;12:5540-8. DOI
40. Lu B, Liu Q, Chen S. Electrocatalysis of single-atom sites: impacts of atomic coordination. *ACS Catal* 2020;10:7584-618. DOI
41. Perdew JP, Burke K, Ernzerhof M. Generalized gradient approximation made simple. *Phys Rev Lett* 1996;77:3865-8. DOI PubMed
42. Kresse G, Furthmüller J. Efficient iterative schemes for *ab initio* total-energy calculations using a plane-wave basis set. *Phys Rev B Condens Matter* 1996;54:11169-86. DOI PubMed
43. Grimme S, Antony J, Ehrlich S, Krieg H. A consistent and accurate *ab initio* parametrization of density functional dispersion correction (DFT-D) for the 94 elements H-Pu. *J Chem Phys* 2010;132:154104. DOI PubMed
44. Zhang C, Qin S, Li B, Jin P. Dual-metal atom incorporated N-doped graphenes as oxygen evolution reaction electrocatalysts: high activities achieved by site synergies. *J Mater Chem A* 2022;10:8309-23. DOI
45. Momma K, Izumi F. *VESTA 3* for three-dimensional visualization of crystal, volumetric and morphology data. *J Appl Cryst* 2011;44:1272-6. DOI
46. Yang TT, Wang A, House SD, Yang J, Lee JK, Saidi WA. Computationally guided design to accelerate discovery of doped β-Mo_2C catalysts toward hydrogen evolution reaction. *ACS Catal* 2022;12:11791-800. DOI
47. Nørskov JK, Rossmeisl J, Logadottir A, et al. Origin of the overpotential for oxygen reduction at a fuel-cell cathode. *J Phys Chem B* 2004;108:17886-92. DOI
48. Hossain MD, Liu Z, Zhuang M, et al. Rational design of graphene-supported single atom catalysts for hydrogen evolution reaction. *Adv Energy Mater* 2019;9:1803689. DOI
49. Hammer B, Norskov JK. Why gold is the noblest of all the metals. *Nature* 1995;376:238-40. DOI
50. Lim J, Back S, Choi C, Jung Y. Ultralow overpotential of hydrogen evolution reaction using Fe-doped defective graphene: a density functional study. *ChemCatChem* 2018;10:4450-5. DOI
51. Yang Y, Zhang H, Liang Z, et al. Role of local coordination in bimetallic sites for oxygen reduction: a theoretical analysis. *J Energy Chem* 2020;44:131-7. DOI
52. Crabtree RH. Dihydrogen complexes: some structural and chemical studies. *Acc Chem Res* 1990;23:95-101. DOI
53. Heinekey DM, Lledŏs A, Lluch JM. Elongated dihydrogen complexes: what remains of the H-H bond? *Chem Soc Rev* 2004;33:175-82. DOI
54. Kubas GJ. Fundamentals of H_2 binding and reactivity on transition metals underlying hydrogenase function and H_2 production and storage. *Chem Rev* 2007;107:4152-205. DOI PubMed
55. Kubas GJ. Molecular hydrogen complexes: coordination of a .sigma. bond to transition metals. *Acc Chem Res* 1988;21:120-8. DOI
56. Crabtree RH. Dihydrogen complexation. *Chem Rev* 2016;116:8750-69. DOI PubMed
57. Alcaraz G, Grellier M, Sabo-Etienne S. Bis sigma-bond dihydrogen and borane ruthenium complexes: bonding nature, catalytic applications, and reversible hydrogen release. *Acc Chem Res* 2009;42:1640-9. DOI PubMed
58. Di Liberto G, Cipriano LA, Pacchioni G. Role of dihydride and dihydrogen complexes in hydrogen evolution reaction on single-atom catalysts. *J Am Chem Soc* 2021;143:20431-41. DOI PubMed PMC
59. Di Liberto G, Cipriano LA, Pacchioni G. Single atom catalysts: what matters most, the active site or the surrounding? *ChemCatChem* 2022;14:e202200611. DOI
60. Wang J, Zhang Z, Song H, et al. Water dissociation kinetic-oriented design of nickel sulfides via tailored dual sites for efficient alkaline hydrogen evolution. *Adv Funct Mater* 2021;31:2008578. DOI